World Journal of Engineering Research and Technology
WJERT
www.wjert.org
SJIF Impact Factor: 5.924

IMPACT OF MOVING OSCILLATING VERTICAL PLATE ON MHD HYBRID NANOFLUID FLOW WITH THERMAL RADIATION

Ch. Sridevi*[1] and A. Sailakumari[2]

[1]Research Scholar, Department of Mathematics, JNTUA College of Engineering Anantapur, A.P.,India.

[2]Department of Mathematics, JNTUA College of Engineering Anantapur, A.P., India.

Article Received on 26/10/2022 **Article Revised on 16/11/2022** **Article Accepted on 06/12/2022**

***Corresponding Author**
Ch. Sridevi
Research Scholar, Department of Mathematics, JNTUA College of Engineering Anantapur, A.P.,India.

ABSTRACT

The current research is focused on the characteristics of Silver-Aluminium oxide/water hybrid nanofluid flow and heat transfer performance due to a moving oscillating plate. In the presence of Lorentz force and radiation parameter effects, we analyse 2D Laminar viscous incompressible boundary layer fluid flow. The governing partial differential equations with accompanying boundary conditions are solved using a robust Crank-Nicolson approach. For specific cases of the problem, the current work is supported by existing literature. The effects of important physical parameters on the skin friction coefficient, Nusselt number, and velocity and temperature profiles are graphically represented. The findings can be applied to the cooling of a variety of engineering and industrial devices.

KEYWORDS: Free convection, oscillating vertical plate, Crank Nicolson numerical technique,laminar boundary layer flow, MHD, thermal radiation.

INTRODUCTION

Nowadays, many researchers have been attracted and showing interest in nanofluids to improve the fluid's heat transfer and thermal conductivity and study the fluid characteristics. Mainly nanofluid applications focus on practical fields, i.e. heat transfer equipment, solar collectors, refrigerators, electronics coolings, nuclear reactor cooling. When compared to liquid particles, solid particles have more thermal conductance. Adding nano- sized solid

particles to liquids improves their thermal conductance, this type of combination is called nanofluids. Rajesh et al.[1-7] have done a wide range of research on nanofluids flows with heat transfer past a moving vertical plate, cylinder with MHD, thermal radiation, viscous dissipation, temperature oscillation, and variable surface temperature effects. Sridevi et al.[8] numerically analysed transient magnetite-water nanofluid flow and heat transfer from a vertical oscillating plate. The transient free convective flow of CNT water nanofluid with heat transfer from a moving cylinder has been studied later by Sridevi et al.[9] Because of many applications, researchers are presently using hybrid-nanofluid instead of nanofluid, which is engineered by dispersing different nanoparticles in mixture form or composite form to increase thermal conductivity. Manjunatha et al.[10] observed a heat transfer enhancementin the boundary layer flow of hybrid nanofluids due to variable viscosity and natural convection. Then, Iskandar Waini et al.[11] explored hybrid nanofluid flow towards a stagnation point on a stretching/shrinking cylinder. Asifa Tassaddiq et al.[12] studied heat and mass transfer and hybrid nanofluid flow over a rotating disk. Ramesh et al.[13] looked at Al2O3-Ag and Al2O3-Cu hybrid nanoparticles' interaction with water on convectively heated moving material. Muhammad et al.[14] Aladdin et al.[15] Mohsan Hassan et al.[16] Huminic et al., [17] Rajesh et al.[18-19] are some of the researchers who examined and extended their work in hybrid nanofluids. Some other helpful studies on hybrid nanofluids are explored in.[20,31]

Because of many applications of hybrid nanofluid flows, we, therefore, investigate the problem of an unsteady boundary-layer flow of a hybrid nanofluid past a moving oscillating plate numerically. This work can be considered as an extension of Rajesh et al.[7]

The novelties of the current study compared to Rajesh et al.[7] include:

i) Hybrid nanofluid ($Ag\ Al_2O_3$) is introduced.
ii) Moving oscillating vertical plate is considered.
iii) Thermal radiation term is taken into account.

The development of the temperature and velocity distributions and engineering quantities like Nusselt number and skin friction coefficient has been exemplified for appropriate parameters: magnetic parameter, radiation parameter, Grashof number, nanoparticle volume fraction and phase angle.

2. Formulation of the problem

In the coordinate system, the x' axis and y' axis are taken along and normal to the plate's surface as shown in Figure 1. In the beginning, both the plate and fluid are kept static at temperature T'_∞ for all $t' \le 0$. Subsequently, at a time $t' > 0$, the plate commences to be in motion vertically with uniform velocity u_0 and oscillates in its plane with a velocity $u_0 \cos(w't')$. Plate surface temperature is elevated to T'_w $(> T'_\infty)$ and retained uniform. We assume that the constant magnetic field with an intensity of B_0 acts in the y'-axis direction and the induced magnetic field consequence is negligible, reasonable when the magnetic Reynolds number is small. The viscous dissipation, Ohmic heating, ion slip, and Hall effects are assumed to be negligible. In the present analysis, silver Ag and aluminium oxide Al_2O_3 nano size particles with water as a base fluid are considered. Initially, in this problem Al_2O_3 /water nanofluid is formed by scattering Al_2O_3 nanoparticles of 0.1 vol. solid volume fraction (which is fixed from beginning to the end of the problem) in the base fluid i.e. water. To form our required hybrid nanofluid $Ag - Al_2O_3$/water, Ag nanoparticles with different volume fractions are dispersed in Al_2O_3/water nanofluid. With Boussinesq's approximation [32] and above assumptions, the transient natural convection boundary layer equations by adopting Tiwari and Das [33] nanofluid model are written as

$$\frac{\partial v_x}{\partial x} + \frac{\partial v_y}{\partial y} = 0 . \tag{1}$$

$$\frac{\partial v_x}{\partial t'} + v_x \frac{\partial v_x}{\partial x} + v_y \frac{\partial v_x}{\partial y} = \nu_{hnf} \frac{\partial^2 v_x}{\partial y^2} + \frac{(\rho\beta)_{hnf}}{\rho_{hnf}} g\left(T' - T'_\infty\right) - \frac{\sigma_{hnf} B_0^2 v_x}{\rho_{hnf}} . \tag{2}$$

$$\frac{\partial T'}{\partial t'} + v_x \frac{\partial T'}{\partial x} + v_y \frac{\partial T'}{\partial y} = \frac{\kappa_{hnf}}{\left(\rho C_p\right)_{hnf}} \frac{\partial^2 T'}{\partial y^2} - \frac{1}{\left(\rho C_p\right)_{hnf}} \frac{\partial q_r}{\partial y} . \tag{3}$$

Where q_r *is r*adiative heat flux and it is defined as

$$q_r = -\frac{4\sigma_s}{3k_e} \frac{\partial T'^4}{\partial y} . \tag{4}$$

Here σ_s and k_e denote the Stefan–Boltzmann constant and coefficient of absorption, respectively. By applying Rosseland approximation, we confined our analysis to optically thick nanofluids. Suppose differences of temperature within the flow are slight such. In that case, that T'^4 may be expressed as a linear function of the temperature, applying Taylor's series for T'^4 about T'_∞ after neglecting higher-order terms as:

$$T'^4 \cong 4T'^3_\infty T' - 3T'^4_\infty . \tag{5}$$

Then we obtain

$$\frac{\partial q_r}{\partial y} = -\frac{16\sigma_s \left(T'_\infty\right)^3}{3k_e}\frac{\partial^2 T'}{\partial y^2} . \tag{6}$$

On considering equations (4), (5) and (6) equation (3) becomes

$$\frac{\partial T'}{\partial t'} + v_x\frac{\partial T'}{\partial x} + v_y\frac{\partial T'}{\partial y} = \frac{\kappa_{hnf}}{\left(\rho C_p\right)_{hnf}}\frac{\partial^2 T'}{\partial y^2} + \frac{16\sigma_s T'^3_\infty}{3k_e\left(\rho C_p\right)_{hnf}}\frac{\partial^2 T'}{\partial y^2} . \tag{7}$$

The initial and boundary conditions are

$t' \le 0 : v_x = 0,\ v_y = 0, T' = T'_\infty$ for all x and y.

$t' > 0 : v_x = u_0 + u_0\cos(w't'), v_y = 0,\ T' = T'_w$ at $y = 0$.

$v_x = 0, T' = T'_\infty$ at $x = 0$.

$v_x \to 0,\ T' \to T'_\infty$ as $y \to \infty$. (8)

The fundamental thermophysical properties of hybrid nanofluid, namely Density ρ_{hnf}, Dynamic viscosity μ_{hnf}, Heat Capacity $(\rho C_P)_{hnf}$, Thermal expansion coefficient $(\rho\beta)_{hnf}$, Thermal Conductivity κ_{hnf}, and Electrical conductivity σ_{hnf} are stated in Table 1. Thermophysical properties of water and nanoparticles are presented in Table 2.

Using the following transformations

$$V_x = \frac{v_x}{u_0},\ V_y = \frac{v_y}{u_0},\ X = \frac{xu_0}{\nu_f} = \frac{x}{L_{ref}},\ Y = \frac{yu_0}{\nu_f} = \frac{y}{L_{ref}},\ t = \frac{t'u_0^2}{\nu_f},\ T = \frac{T' - T'_\infty}{T'_w - T'_\infty},\ \omega = \frac{\omega'\nu_f}{u_0^2} . \tag{9}$$

into equations (1), (2) and (7) we get

$$\frac{\partial V_x}{\partial X} + \frac{\partial V_y}{\partial Y} = 0 . \tag{10}$$

$$\frac{\partial V_x}{\partial t} + V_x\frac{\partial V_x}{\partial X} + V_y\frac{\partial V_x}{\partial Y} = \frac{E_2}{E_1}\frac{\partial^2 V_x}{\partial Y^2} + \frac{E_3}{E_1}GrT - \frac{E_4}{E_1}MV_x . \tag{11}$$

$$\frac{\partial T}{\partial t} + V_x\frac{\partial T}{\partial X} + V_y\frac{\partial T}{\partial Y} = \left(\frac{E_6}{E_5} + \frac{4}{3NE_5}\right)\frac{1}{P_r}\frac{\partial^2 T}{\partial Y^2} . \tag{12}$$

The corresponding initial and boundary conditions are

$t \le 0 :\ V_x = 0, V_y = 0, T = 0$ for all X and Y.

$$t>0: V_x = 1+\cos\omega t\,,\ V_y = 0\,,\ T = 1 \quad \text{at} \quad \text{Y=0.}$$

$$V_x = 0,\ T = 0 \ \text{at} \qquad \text{X=0}\,.$$

$$V_x \to 0, T \to 0 \ \text{as} \ \ Y \to \infty\,. \tag{13}$$

Where

$\text{Pr} = \dfrac{\nu_f}{\alpha_f}$ (Prandtl number), $G_r = \dfrac{g\beta_f \nu_f \left(T'_w - T'_\infty\right)}{u_0^3}$ (Grashof number), $M = \dfrac{\sigma_f B_0^2\, \nu_f}{\rho_f u_0^2}$ (Magnetic parameter), $N = \dfrac{k_f k_e}{4\sigma_s T'^3_\infty}$ (Radiation parameter) and

$$E_1 = [(1-\phi_2)\{(1-\phi_1)+\phi_1\frac{\rho_{s1}}{\rho_f}\}]+\phi_2\frac{\rho_{s2}}{\rho_f},$$

$$E_2 = \frac{1}{(1-\phi_1)^{2.5}(1-\phi_2)^{2.5}},$$

$$E_3 = [(1-\phi_2)\{(1-\phi_1)+\phi_1\frac{(\rho\beta)_{s1}}{(\rho\beta)_f}\}]+\phi_2\frac{(\rho\beta)_{s2}}{(\rho\beta)_f},$$

$$E_4 = \frac{\sigma_{bf}}{\sigma_f}\left[\frac{\sigma_{s2}(1+2\phi_2)+2\sigma_{bf}(1-\phi_2)}{\sigma_{s2}(1-\phi_2)+\sigma_{bf}(2+\phi_2)}\right],$$

$$E_5 = [(1-\phi_2)\{(1-\phi_1)+\phi_1\frac{(\rho C_p)_{s1}}{(\rho C_p)_f}\}]+\phi_2\frac{(\rho C_p)_{s2}}{(\rho C_p)_f},$$

$$E_6 = \frac{\kappa_{bf}}{\kappa_f}\frac{\left[\kappa_{s2}+(n_1-1)\kappa_{bf}-(n_1-1)\phi_2(\kappa_{bf}-\kappa_{s2})\right]}{\left[\kappa_{s2}+(n_1-1)\kappa_{bf}+\phi_2(\kappa_{bf}-\kappa_{s2})\right]}. \tag{14}$$

The exact solution of Eq. (12) in the absence of inertial terms and thermal radiation, subject to the boundary conditions (13) by using the Laplace transform method, is given by

$$T = erfc\left(\frac{Y\sqrt{\text{Pr}}}{2\sqrt{\left(\frac{E_6}{E_5}\right)t}}\right). \tag{15}$$

3. The skin friction coefficient and Nusselt number

The quantities of practical interest in this study are the skin friction coefficient C_f and the local Nusselt number Nu , which are defined as the following:

$$C_f = \frac{\tau_w}{\rho_f u_0^2}, \qquad Nu = \frac{q_w L_{ref}}{\kappa_f (T_w' - T_\infty')}. \tag{16}$$

Here τ_w is the skin-friction (or shear stress), and q_w is the heat flux (or the rate of heat transfer) from the surface of the plate, and they are given by:

$$\tau_w = \mu_{hnf}\left(\frac{\partial v_x}{\partial y}\right)_{y=0}, \quad q_w = -\kappa_{hnf}\left(\frac{\partial T'}{\partial y}\right)_{y=0}. \tag{17}$$

Using non-dimensional variables (9), we get

$$C_f = \frac{1}{(1-\phi_1)^{2.5}(1-\phi_2)^{2.5}}\left(\frac{\partial V_x}{\partial Y}\right)_{Y=0}, \qquad Nu = -\frac{\kappa_{hnf}}{\kappa_f}\left(\frac{\partial T}{\partial Y}\right)_{Y=0}. \tag{18}$$

4. Numerical Technique

The PDEs (10)-(12) together with appropriate conditions (13) have been solved by a robust Crank-Nicolson type implicit finite-difference technique. The corresponding finite-difference equations are

$$\left[\frac{(V_x)_{i,j}^{n+1} - (V_x)_{i-1,j}^{n+1} + (V_x)_{i,j}^{n} - (V_x)_{i-1,j}^{n} + (V_x)_{i,j-1}^{n+1} - (V_x)_{i-1,j-1}^{n+1} + (V_x)_{i,j-1}^{n} - (V_x)_{i-1,j-1}^{n}}{4\Delta X}\right]$$
$$+\left[\frac{(V_y)_{i,j}^{n+1} - (V_y)_{i,j-1}^{n+1} + (V_y)_{i,j}^{n} - (V_y)_{i,j-1}^{n}}{2\Delta Y}\right] = 0 \tag{19}$$

$$\left[\frac{(V_x)_{i,j}^{n+1} - (V_x)_{i,j}^{n}}{\Delta t}\right] + (V_x)_{i,j}^{n}\left[\frac{(V_x)_{i,j}^{n+1} - (V_x)_{i-1,j}^{n+1} + (V_x)_{i,j}^{n} - (V_x)_{i-1,j}^{n}}{2\Delta X}\right]$$
$$+(V_Y)_{i,j}^{n}\left[\frac{(V_x)_{i,j+1}^{n+1} - (V_x)_{i,j-1}^{n+1} + (V_x)_{i,j+1}^{n} - (V_x)_{i,j-1}^{n}}{4\Delta Y}\right]$$
$$= \frac{E_3}{E_1}\frac{G_r}{2}\left[T_{i,j}^{n+1} + T_{i,j}^{n}\right] + \frac{E_2}{E_1}\left[\frac{(V_x)_{i,j-1}^{n+1} - 2(V_x)_{i,j}^{n+1} + (V_x)_{i,j+1}^{n+1} + (V_x)_{i,j-1}^{n} - 2(V_x)_{i,j}^{n} + (V_x)_{i,j+1}^{n}}{2(\Delta Y)^2}\right]$$
$$-\frac{E_4}{E_1}\frac{M}{2}\left[(V_x)_{i,j}^{n+1} + (V_x)_{i,j}^{n}\right] \tag{20}$$

$$\left[\frac{T_{i,j}^{n+1}-T_{i,j}^{n}}{\Delta t}\right]+(V_x)_{i,j}^{n}\left[\frac{T_{i,j}^{n+1}-T_{i-1,j}^{n+1}+T_{i,j}^{n}-T_{i-1,j}^{n}}{2\Delta X}\right]+(V_y)_{i,j}^{n}\left[\frac{T_{i,j+1}^{n+1}-T_{i,j-1}^{n+1}+T_{i,j+1}^{n}-T_{i,j-1}^{n}}{4\Delta Y}\right]$$
$$=\left(\frac{E_6}{E_5}+\frac{4}{3NE_5}\right)\left[\frac{T_{i,j-1}^{n+1}-2T_{i,j}^{n+1}+T_{i,j+1}^{n+1}+T_{i,j-1}^{n}-2T_{i,j}^{n}+T_{i,j+1}^{n}}{2\Pr(\Delta Y)^2}\right] \quad (21)$$

The above equations are solved for the numerical solutions of temperature and velocity fields via the Thomas algorithm. More details of solving these equations containing stability and convergence have been elaborated by Muthukumaraswamy and Ganesan [34], Ramachandra Prasad et al.[35] A grid-independent test has been conducted to obtain an economical and reliable grid system for the computations and noted that the step sizes Δx=0.05 and Δy=0.25 are giving accurate results. Also, the time step size dependency has been carried out, from which Δt = 0.01 was observed to provide a reliable product. Further to check the numerical results rightness, the temperature profiles of the present study in the absence of thermal radiation when are compared with the analytical solution given by equation (15) in.

Figure 2 and proven to be in perfect agreement. Further, the present results (when $\omega t=\frac{\pi}{2}$, $\phi_2=0$) in the absence of thermal radiation have been compared with results of Rajesh et al. [7] in table 3 and found to be in excellent agreement. This agreement confirms that the present numerical technique is fit for this type of problem.

Table 1. Thermophysical properties of $Ag-Al_2O_3$/water.

Property	Hybrid nanofluid ($Ag-Al_2O_3$/water)
Density	$\rho_{hnf}=[(1-\phi_2)\{(1-\phi_1)\rho_f+\phi_1\rho_{s1}\}]+\phi_2\rho_{s2}$
Dynamic viscosity	$\mu_{hnf}=\frac{\mu_f}{(1-\phi_1)^{2.5}(1-\phi_2)^{2.5}}$
Heat Capacity	$(\rho C_P)_{hnf}=[(1-\phi_2)\{(1-\phi_1)(\rho C_P)_f+\phi_1(\rho C_P)_{s1}\}]+\phi_2(\rho C_P)_{s2}$
Thermal expansion coefficient	$(\rho\beta)_{hnf}=[(1-\phi_2)\{(1-\phi_1)(\rho\beta)_f+\phi_1(\rho\beta)_{s1}\}]+\phi_2(\rho\beta)_{s2}$
Thermal Conductivity	$\kappa_{hnf}=\kappa_{bf}\frac{\kappa_{s2}+(n_1-1)\kappa_{bf}-(n_1-1)\phi_2(\kappa_{bf}-\kappa_{s2})}{\kappa_{s2}+(n_1-1)\kappa_{bf}+\phi_2(\kappa_{bf}-\kappa_{s2})}$, where $\kappa_{bf}=\kappa_f\frac{\kappa_{s1}+(n_1-1)\kappa_f-(n_1-1)\phi_1(\kappa_f-\kappa_{s1})}{\kappa_{s1}+(n_1-1)\kappa_f+\phi_1(\kappa_f-\kappa_{s1})}$
Electrical conductivity	$\sigma_{hnf}=\sigma_{bf}\left[\frac{\sigma_{s2}(1+2\phi_2)+2\sigma_{bf}(1-\phi_2)}{\sigma_{s2}(1-\phi_2)+\sigma_{bf}(2+\phi_2)}\right]$, where $\sigma_{bf}=\sigma_f\left[\frac{\sigma_{s1}(1+2\phi_1)+2\sigma_f(1-\phi_1)}{\sigma_{s1}(1-\phi_1)+\sigma_f(2+\phi_1)}\right]$

Table 2. Thermophysical properties of water and nanoparticles

	$\rho(kg/m^3)$	$C_p(J/kgK)$	$\kappa(W/mK)$	$\sigma(s/m)$	$\beta(1/K)$
H_2O (f)	997.1	4179	0.613	5.5×10^{-6}	21×10^{-5}
Al_2O_3 $(s1)$	3970	765	40	35×10^{6}	0.85×10^{-5}
Ag $(s2)$	10500	235	429	6.30×10^{7}	1.89×10^{-5}

5. RESULTS AND DISCUSSION

Numerical results are obtained by solving the equations (10-12) by using the crank Nicolson type implicit finite difference method. Effects of apposite physical parameters namely Magnetic parameter (M), Grashof number (Gr), Radiation parameter (N), Phase angle (ωt), Nanoparticle volume fraction (ϕ_2), on the velocity with t and y, temperature with t and

y, skin friction coefficient with x, Nusselt number with x are delineated through figures (3-32). Table 1 gives us standard thermophysical properties of $Ag-Al_2O_3$/water.

Table 3. Comparison of Nusselt number (when $\omega t=\frac{\pi}{2}$, $\phi_2=0$) in the absence of thermal radiation at Pr=6.2, M=5, Gr=2, X=1, and t=1.0.

	Al2O3/water	
ϕ_1	Rajesh et al. [7]	Present result
0	1.4280	1.4280
0.01	1.4452	1.4452
0.02	1.4626	1.4626
0.03	1.4801	1.4801
0.04	1.4977	1.4977

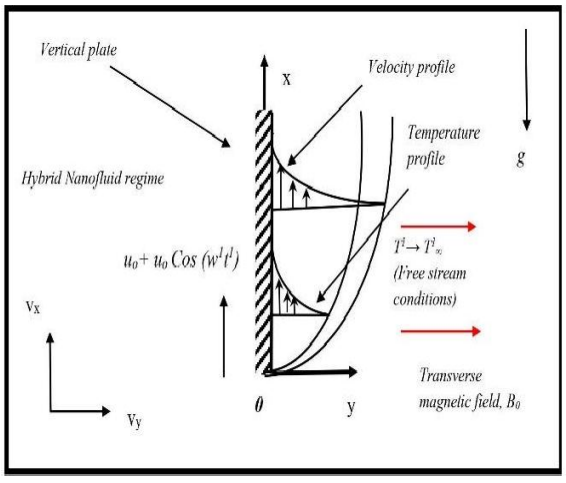

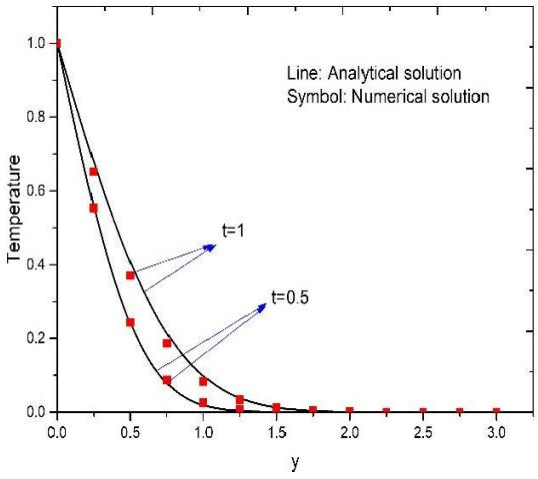

Fig. 1: The physical model and coordinate system. Fig. 2: Comparison of temperature profiles.

It is predictable from figures 3 & 4 that magnetic parameter M diminishes the velocity concerning time and distance. Generally, high values of M augment Lorentz force, which opposes the fluid flow. For M=0, Al_2O_3/water has a higher velocity than $Ag-Al_2O_3$/water. The same thing observed for M=5, 10 with respect time, whereas concerning y for M=5,10 both the liquids show a slight difference between them. Initially, velocity increases with time, after reaching a particular point both the fluids get to steady-state. It is observed from figure 5 & 6 that, as M increase, the temperature with t and y of both the nanofluid and hybrid nanofluids increase. This increase in temperature for $Ag-Al_2O_3$/water is more when compared with Al_2O_3/water. In figures 7 & 8, the skin friction coefficient and Nusselt number decrease with the increases in the magnetic parameter for $Ag-Al_2O_3$/water and Al_2O_3/water. Nanofluid values are more than hybrid nanofluid in the skin friction coefficient, whereas in Nusselt number, the opposite trend in values noted with a slight difference between liquids.

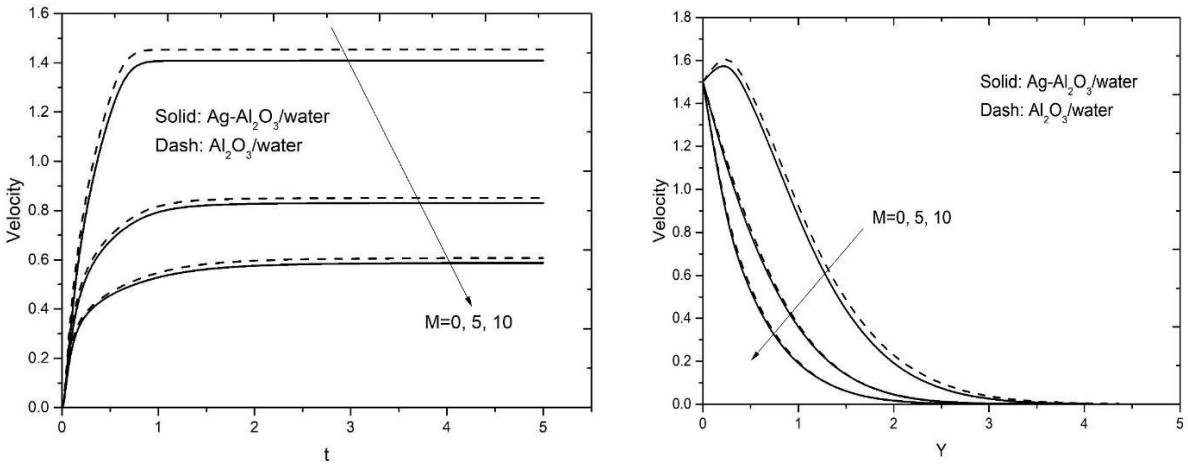

Fig. 3: Impact of M on velocity with t. Fig. 4: Impact of M on velocity with y.

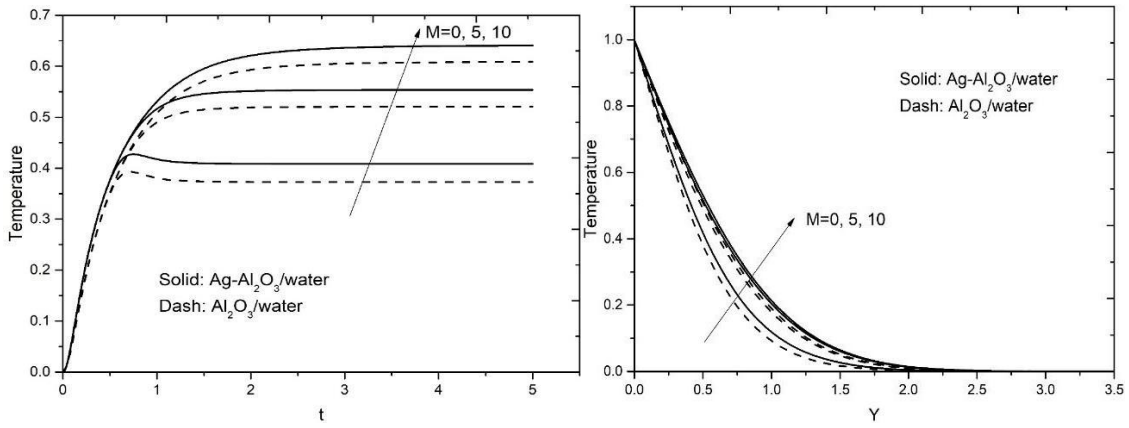

Fig. 5: Impact of M on temperature with t. Fig. 6: Impact of M on temperature with y.

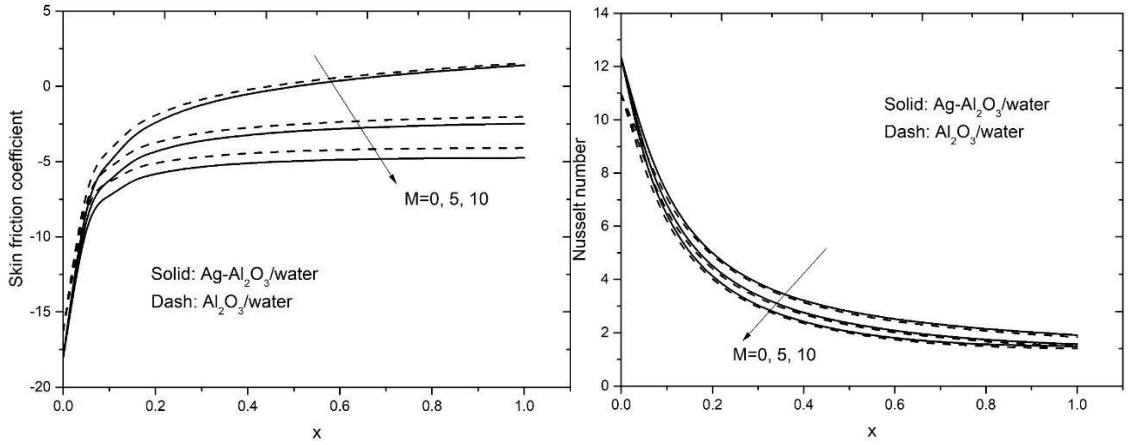

Fig. 7: Impact of M on skinfriction coeff with x. Fig. 8: Impact of M on Nusselt number with x.

Grashof number Gr's impact on the velocity with time & distance has been exposed in figure 9 and figure10. It is evident from the plots that the rising values of Gr augmented the velocity with t and y and observed that hybrid nanofluid has less velocity than nanofluid. In temperature profiles from figures 11 & 12, both the liquids $Ag-Al_2O_3$/water and Al_2O_3/H_2O decrease with increase in Gr concerning time t and distance y and noticed that both the liquids initially rise to a certain level and reach steady state. Figure 13 portrayed for variation of the skin friction coefficient against Gr; it is observed that the skin friction coefficient is highest for Al_2O_3/water than $Ag-Al_2O_3$/water. Figure 14 exhibited the effect of Gr on the local Nusselt number. It noted that there is no significant difference between the Nusselt number's values of nanofluid and hybrid nanofluid.

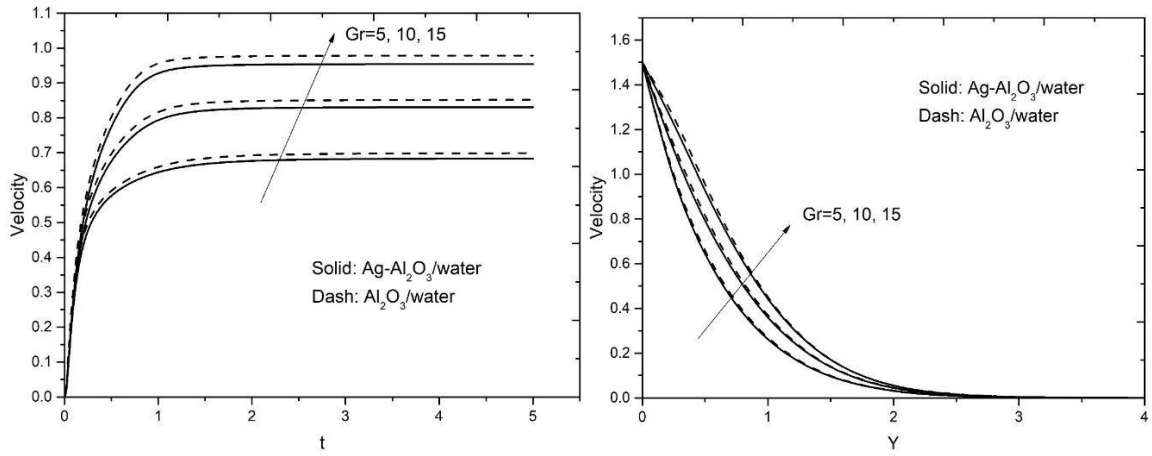

Fig. 9: Impact of Gr on velocity with t. Fig. 10: Impact of Gr on velocity with y.

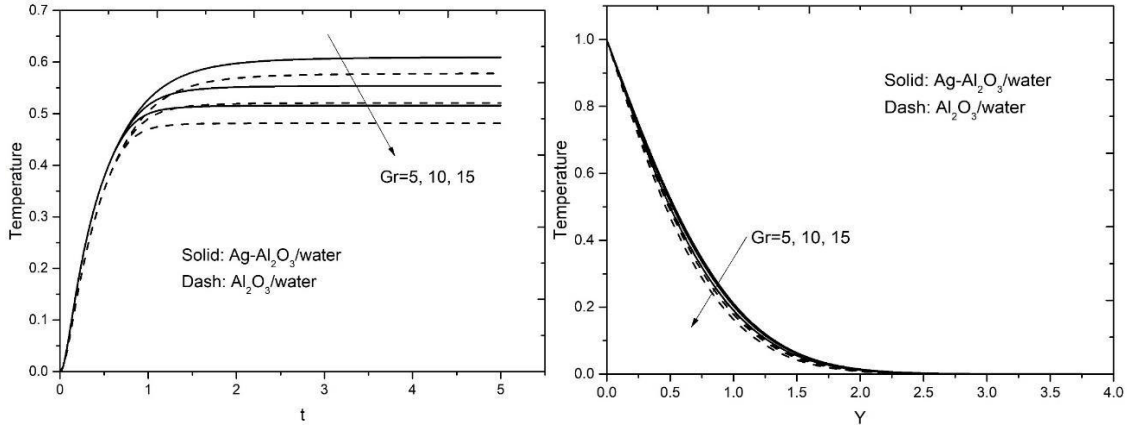

Fig. 11: Impact of Gr on temperature with t. Fig. 12: Impact of Gr on temperature with y.

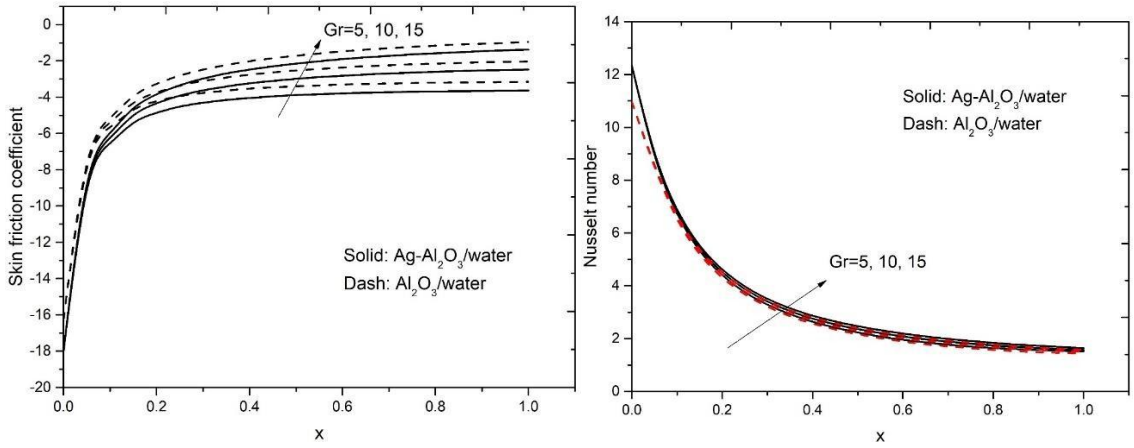

Fig. 13: Impact of Gr on skinfriction coeff with x. Fig. 14: Impact of Gr on Nusselt num with x.

Figures 15 and 16 show the effect of thermal radiation parameter N on the velocitywith t and y. As radiation parameter increases correspondingly, velocity decreases for both.

nanofluid and hybrid nanofluid, and also observed that nanofluid has more velocity than hybrid nanofluid with an increase of radiation parameter. Same way noticed in figures 17 and 18 that temperature with t and y decreases for increasing radiation parameter, but here $Ag - Al_2O_3$/water shows an increase in temperature than Al_2O_3/water concerning t and y. Skin friction coefficient decreases with an increase in N(radiation parameter) from figure 19 and Al_2O_3/water show more skin friction effects than $Ag - Al_2O_3$/water. Figure 20 shows that the Nusselt number increases with an increase in radiation parameter in nanofluid and hybrid nanofluid, and perceived Al_2O_3/water shows minor Nusselt number effects than $Ag - Al_2O_3$/water.

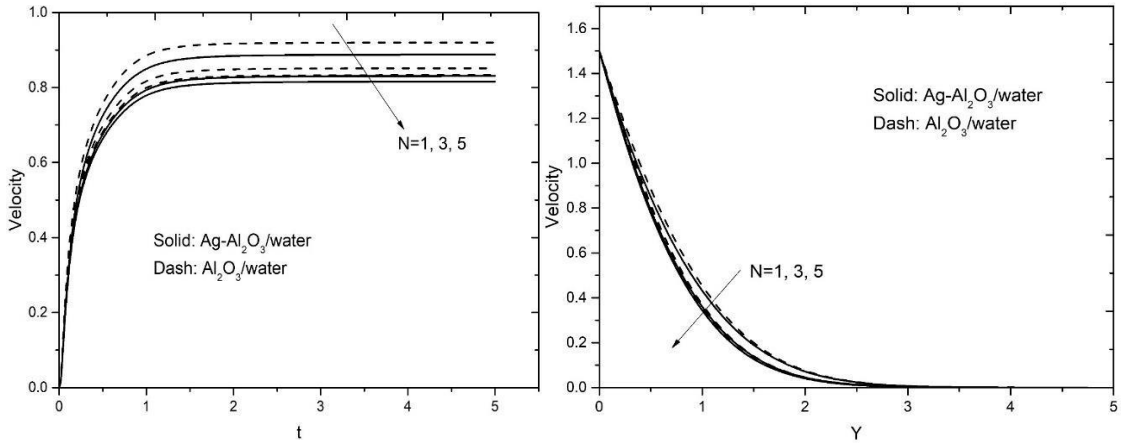

Fig. 15: Impact of N on velocity with t. Fig. 16: Impact of N on velocity with y.

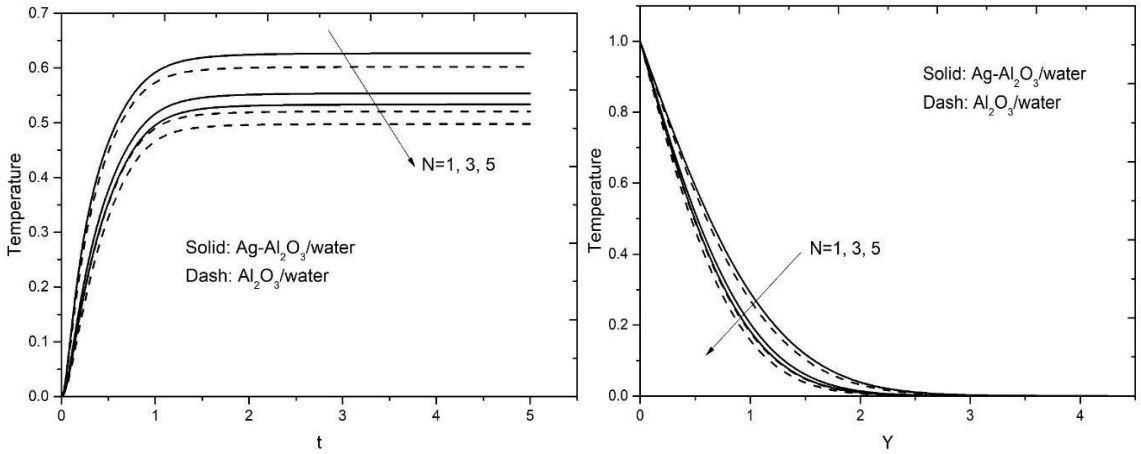

Fig. 17: Impact of N on temperature with t. Fig. 18: Impact of N on temperature with y.

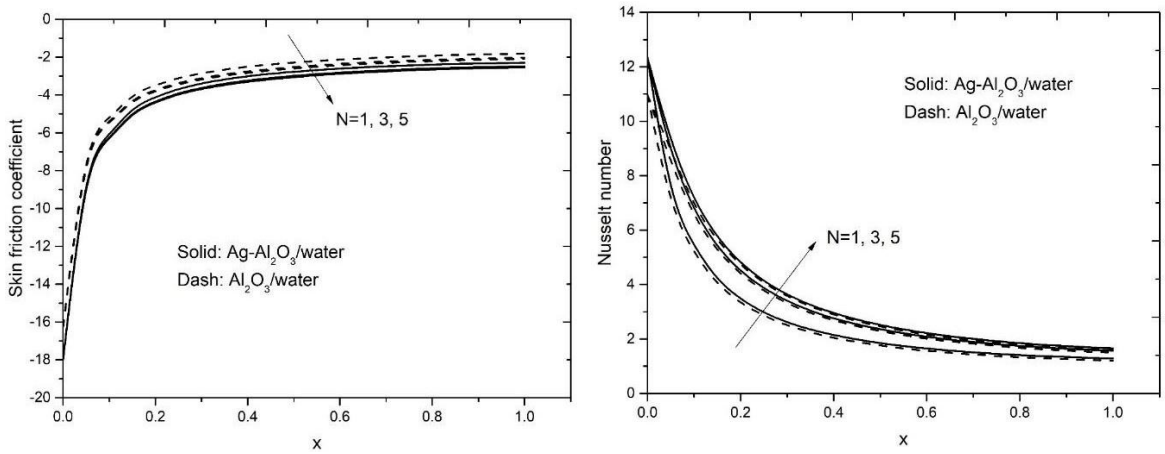

Fig. 19: Impact of N on skinfriction coeff with x. Fig. 20: Impact of N on Nusseltnum with x.

Figures 21 and 22 show the behaviour of velocity distribution with increasing phase angle (ωt). It falls with a rise of phase angle(ωt), and nanofluid has more velocity than hybrid nanofluid concerning t & y. The effect ωt on temperature concerning t and y is shown in figures 23 & 24. temperature increases with the increase in phase angle in both nanofluid and hybrid nanofluid, and also espied $Ag-Al_2O_3$/water has more temperature distribution than Al_2O_3/water. Figures 25 and 26 reveal result on C_f and Nu_x for different values of ωt. Skin friction coefficient increases with an increase in ωt, whereas Nusselt number decreases with the rise in ωt for both $Ag-Al_2O_3$/water and Al_2O_3/water.

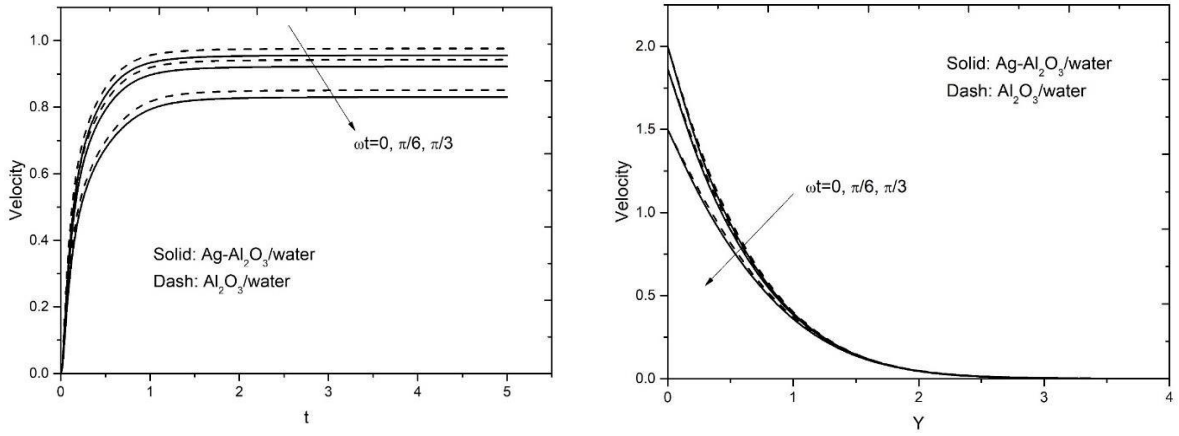

Fig. 21: Impact of ωt on velocity with t. Fig. 22: Impact of ωt on velocity with y.

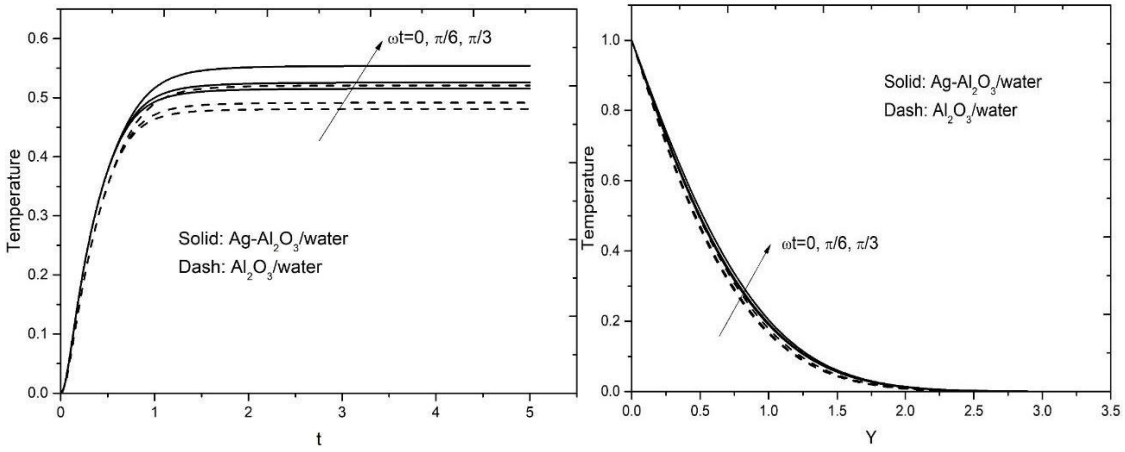

Fig. 23: Impact of ωt on temperature with t. Fig. 24: Impact of ωt on temperature with y.

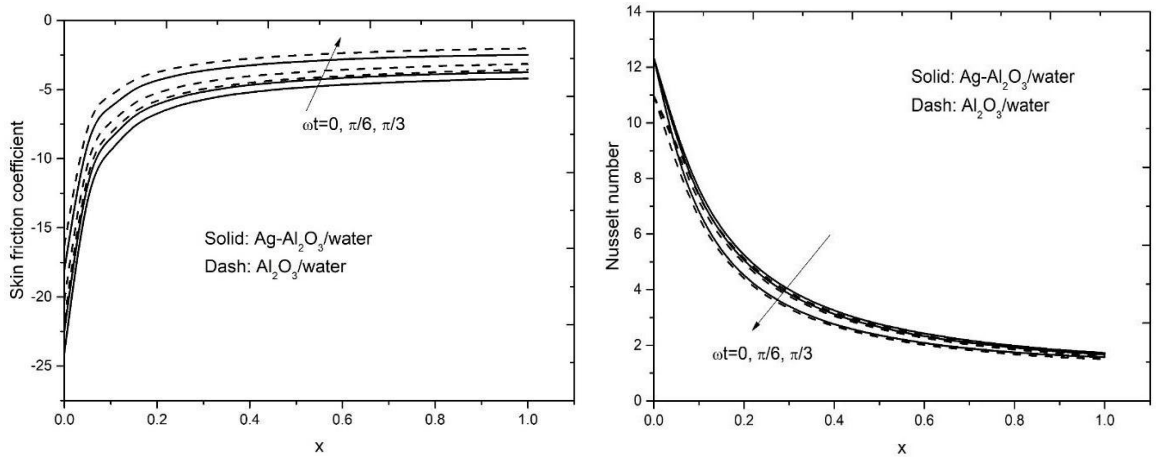

Fig. 25: Impact of ωt on skinfriction coeff with x. Fig. 26: Impact of ωt on Nusseltnum with x.

The impact of ϕ_2 (volume fraction) on velocity for t and y are shown in figure 27 and 28. It is seen that augmentation in volume fraction decreases velocity. The opposite impact is found in temperature for t and y from figures 29, and 30; that is, an increase in volume fraction enhances the temperature profiles. Here increasing rate is slower for Al_2O_3/water than the $Ag-Al_2O_3$/water, which shows that the thermal capability of hybrid nanofluid is better than nanofluid. Figure 31, 32 present the skin friction coefficient and Nusselt number variations with ϕ_2 effects. We observed that the skin friction coefficient decreases with the increment of volume fraction for both nanofluid and hybrid nanofluid. Nussselt number increases with the increment of volume fraction. It is also observed that the local Nusselt number is highest for hybrid nanofluid ($Ag-Al_2O_3$/water) than nanofluid (Al_2O_3/water). High thermal conductivity enhances the Nusselt number because the heat transfer coefficient is proportional to thermal conductivity.

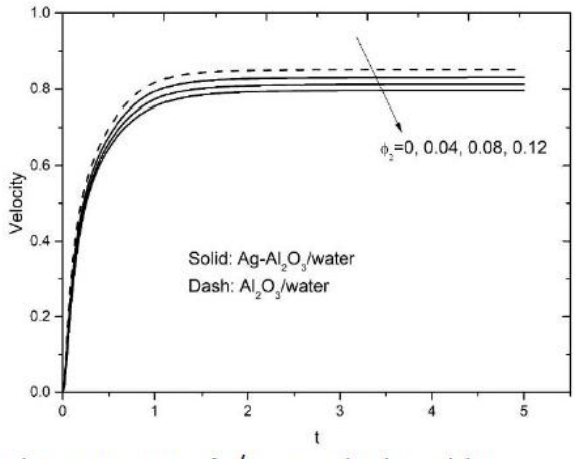

Fig27. Impact of ϕ_2 on velocity with t

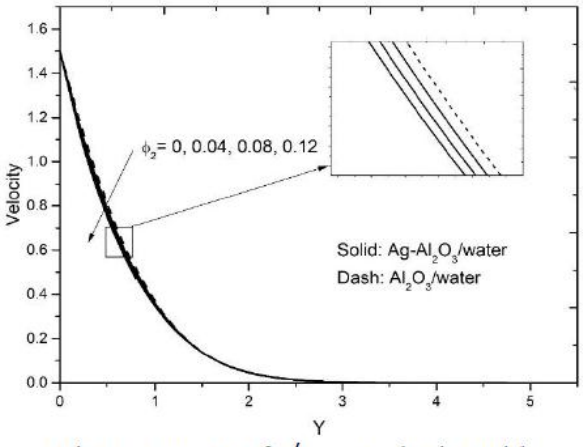

Fig28. Impact of ϕ_2 on velocity with y

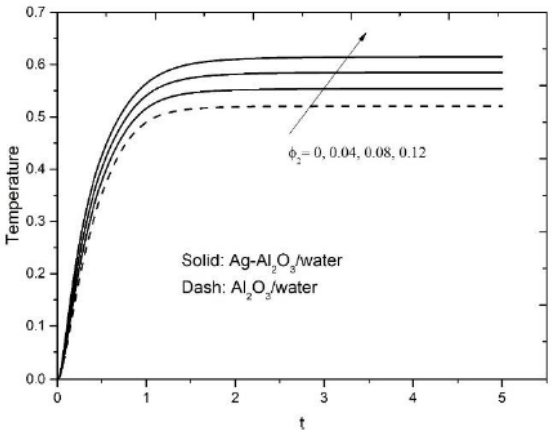

Fig29. Impact of ϕ_2 on temperature with t

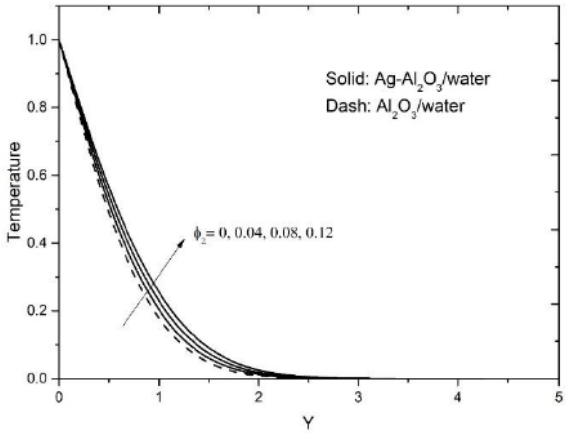

Fig30. Impact of ϕ_2 on temperature with y

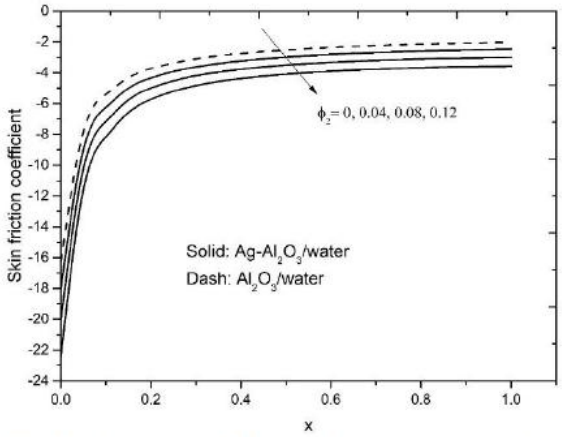

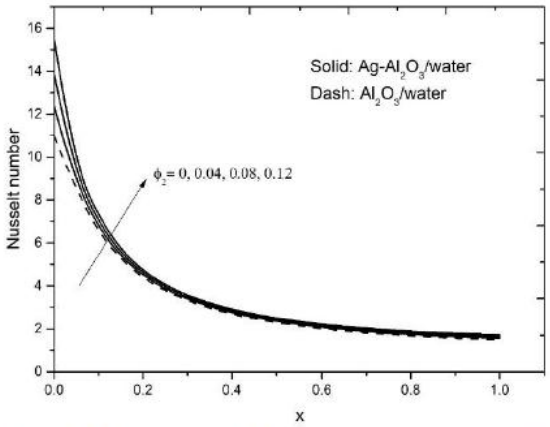

Fig31. Impact of ϕ_2 on skinfriction coeff with x Fig32. Impact of ϕ_2 on Nusseltnum with x

6. CONCLUSIONS

This paper numerically investigated MHD and thermal radiation's impacts on the unsteady boundary-layer flow of a hybrid nanofluid past a moving oscillating plate using the Crank-Nicolson technique. The conclusions of the study are as follows.

1. Increasing M's values leads to augmentation in temperature but drop in velocity, skin friction coefficient and Nusselt number for both nanofluid and hybrid nanofluids.
2. Rising values of Gr demotes temperature profiles but promotes velocity, skin friction coefficient and Nusselt number for both $Ag - Al_2O_3$/water and Al_2O_3/water.
3. Increasing values of N (radiation parameter) increases Nusselt number but decreases velocity, temperature, and skin friction coefficient for both nanofluid and hybrid nanofluids.
4. The temperature and skin friction coefficient significantly increase with an increase in phase angle, relegated in velocity, Nusselt number for both $Ag - Al_2O_3$/water, and Al_2O_3/water.
5. The growing value of volume fraction promotes temperature and Nusselt number but downgrades velocity, skin friction coefficient for nanofluid and hybrid nanofluids.

REFERENCES

1. Rajesh,V., Chamka., Mallesh., M.P., Nanofluid flow past an impulsively started vertical plate with variable surface temperature, International Journal of Numerical Methods for Heat and fluid flow, 2016; 26(1): 328-347.
2. Rajesh,V., Anwar Beg.O., Mallesh. M.P., Transient nanofluid flow and heat transfer from a moving vertical cylinder in the presence of thermal radiation, Numerical study. Proceedings of the Institution of Mechanical Engineers, Part N: Journal of Nano engineering and Nano systems September 5, 2014. DOI:10.1177/1740349914548712.
3. Rajesh, V., Chamkha, A.J., Sridevi, Ch.; Al-Mudhaf, A.F., A numerical investigation of transient MHD free convective flow of a nanofluid over a moving semi-infinite vertical cylinder, Engineering Computations, 2017; 34: 5,1393-1412.
4. Rajesh, V., Anwar, B., O., MHD transient nanofluid flow and heat transfer from a moving vertical cylinder with temperature oscillation, Computat Therm Sci., 2014; 6(5): 439-450.
5. Rajesh, V., Mallesh, MP., Sridevi C., Transient MHD nanofluid flow and heat transferdue to a moving vertical plate with thermal radiation and temperature oscillation effects, Procedia Eng., 2015; 127: 901-908.
6. Rajesh, V., Mallesh, MP., Anwar, BO., Transient MHD free convection flow andheat transfer of nanofluid past an impulsively started vertical porous plate in the presence of viscous dissipation, Procedia Mater Sci., 2015b; 80: 10-89.
7. Rajesh V., Chamkha AJ, Mallesh MP. Transient MHD free convection flow and heat transfer of nanofluid past an impulsively started semi-infinite plate. Journal of Applied Fluid Mechanics, 2016b; 9(5): 2457-2467.
8. Sridevi, Ch., sailakumari, A., Transient magnetite-water nanofluid flow and heat transfer from a vertical oscillating plate, AIP Conference Proceedings, 2020; 2246: 020067. https://doi.org/10.1063/5.0014421.
9. Sridevi, Ch., sailakumari, A., Transient Free Convective Flow Of CNT Water Nanofluid With Heat Transfer From A Moving Cylinder, Nanoscience And Nanotechnology-asia, 2020, DOI : 10.2174/2210681210999200917113354.
10. Manjunatha, S., Kuttan, B., Jayanthi, S., Chamkha, A., Gireesha, B., Heat transfer enhancement in the boundary layer flow of hybrid nanofluids due to variable viscosityand natural convection, Heliyon, 2019; 5(4): e01469. DOI: https://doi.org/10.1016/j. heliyon.2019.e01469.
11. Iskandar Waini, Anuar Ishak, Ioan Pop, Hybrid nanofluid flow towards a stagnation point on a stretching/shrinking cylinder, Scientific Reports, 2020; 10: 9296. |

https://doi.org/10.1038/s41598-020-66126-2.

12. Asifa Tassaddiq, Sadam Khan, Muhammad Bilal, Taza Gul, Safyan Mukhtar, Zahir Shah, Ebenezer Bonyah, Heat and mass transfer together withhybrid nanofluid flow over a rotating disk, AIP Advances, 2020; 10: 055317. https://doi.org/10.1063/5.0010181.
13. Ramesh, G.K., Roopa, G.S., Shehzad, S., Khan, S.U., Interaction of Al_2O_3-Ag and Al_2O_3-Cu hybrid nanoparticles with water on convectively heated moving material, Multidiscipline Modeling in Materials and Structures, 2020; 16(6): 1651-1667. https://doi.org/10.1108/MMMS-11-2019-0191.
14. Muhammad K, Hayat T, Alsaedi, A, Ahmad B., Melting heat transfer in squeezing flow of basefluid (water), nanofluid (CNTs + water) and hybrid nanofluid (CNTs + CuO + water), Journal of Thermal Analysis and Calorimetry, 2020; 143(1115/1). DOI: 10.1007/s10973-020-09391-7.
15. Aladdin N, Bachok, N., Pop I, Cu-Al_2O_3/water hybrid nanofluid flow over a permeable moving surface in presence of hydromagnetic and suction effects. Alexandria Engineering Journal, 2020, 657-666, 59(2), DOI: 10.1016/j.aej.2020.01.028.
16. Mohsan Hassan, Abrar Faisal, Irfan Ali, Muhammad Mubashir Bhatti, Muhammad Yousaf, Effects of Cu–Ag hybrid nanoparticles on the momentum and thermal boundary layer flow over the wedge, Proceedings of the Institution of Mechanical Engineers, Part E: Journal of Process Mechanical Engineering, 2019, 233(5) https://doi.org/10.1177/0954408919844668.
17. Huminic G, Huminic A., Hybrid nanofluids for heat transfer applications – A state-of-the-art review, International Journal of Heat and Mass Transfer, 2018, 82-103, 125.
18. Rajesh Vemula, M. Kavitha, Mikhail A Sheremet, Effects of internal heat generationand Lorentz force on unsteady hybrid nanoliquid flow andheat transfer along a moving plate with nonuniform temperature, Wiley Heat transfer, 2020 https://doi.org/10.1002/htj.22014.
19. Vemula Rajesh, Ali Chamkha, M Kavitha, Numerical investigation of Ag-CuO/water hybrid nanofluid flow past a moving oscillating cylinder with heat transfer, Wiley Mathematical methods in applied sciences, 2020 https://doi.org/10.1002/mma.6884.
20. Rakesh K., Bumataria , N.K. Chavda, Hitesh Panchal, Current research aspects in mono and hybrid nanofluid based heat pipe technologies, Heliyon, 2019,Volume 5, Issue 5, e01627 https://doi.org/10.1016/j.heliyon.2019.e01627.
21. Hayat T, Nadeem S, Khan AU., Rotating flow of Ag-CuO/H_2O hybrid nanofluid with

radiation and partial slip boundary effects, Eur Phys J., 2018, E41(6):75.

22. Dinarvand S, Rostami MN, Pop I., A novel hybridity model for TiO2-CuO/water hybrid nanofluid flow over a static/moving wedge or corner, Science Reports, 2019, 9:16290.
23. Waini I, Ishak A, Pop I., Hybrid nanofluid flow induced by an exponentially shrinking sheet, Chin J Phys, 2019, 68:468-482,https://doi.org/10.1016/j.cjph.2019.12.015.
24. Aly EH, Pop I., MHD flow and heat transfer over a permeable stretching/shrinking sheet in a hybrid nanofluid with a convective boundary condition, Int J Num Methods Heat Fluid Flow, 2019, 29(9):3012-3038.
25. Yahaya RI, Arifin NM, Nazar R, Pop I., Flow and heat transfer past a permeable stretching/shrinking sheet in Cu-Al2O3/water hybrid nanofluid, Int J Num Method Heat Fluid Flow, 2019, 30(3):1197-1222.
26. Ghalambaz M, Sheremet MA, Mehryan SAM, Kashkooli FM, Pop I., Local non-equilibrium analysis of conjugate free convection within a porous enclosureoccupied with Ag-MgO hybrid nanofluid, J Therm Anal Calorim, 2019, 135:1381-1398.
27. Chamkha AJ, Miroshnichenko IV, Sheremet MA., Numerical analysis of unsteady conjugate natural convection of hybrid water-based nanofluid in a semicircular cavity, J Therm Sci Eng Appl, 2017, 9(4):041004. https://doi.org/10.1115/1.4036203.
28. Ghadikolaei SS, Hosseinzadeh K, Ganji DD., Investigation on ethylene glycol-water mixture fluid suspend by hybrid nanoparticles (TiO2- CuO) over rotating cone with considering nanoparticles shape factor, J Mol Liq. 2018,272(15): 226-236.
29. Ashorynejad HR, Shahriari A., MHD natural convection of hybrid nanofluid in an open wavy cavity, Respir Physiol, 2018, 9:440-455.
30. Mashayekhi R, Khodabandeh E, Akbari OA, Toghraie D, Bahiraei M, Gholami M., CFD analysis of thermal and hydrodynamic characteristics of hybrid nanofluid in a new designed sinusoidal double-layered microchannel heat sink, J Therm Anal Calorim, 2018, 134 (3):2305-2315.
31. Pordanjani AH, Vahedi SM, Aghakhani S, Afrand M, Öztop HF, Abu-Hamdeh N., Effect of magnetic field on mixed convection and entropy generation of hybrid nanofluid in an inclined enclosure: sensitivity analysis and optimisation, Eur Phys J Plus, 2019, 134:412.
32. Schlichting, H., Gersten, K., Boundary layer theory, Springer-Verlag, New York, NY2001.
33. Tiwari, R.K., Das, M.K., Heat transfer augmentation in a two-sided lid-driven differentially heated square cavity utilising nanofluids, International Journal of Heat and

Mass Transfer, 2007, 50, 9-10.

34. R. Muthukumaraswamy, P. Ganesan, Unsteady flow past an impulsively started vertical plate with heat and mass transfer, Heat and Mass Transfer 34 (1998) 187-193.
35. Ramachandra Prasad, V.; Bhaskar Reddy, N. Muthucumaraswamy, R., Radiation and mass transfer effects on two-dimensional flow past an impulsively started infinite vertical plate, International Journal of Thermal Science, 2007, 46, 12, 1251-1258.